ELECTRIC ENERGY METERING ERROR EVALUATION METHOD BASED ON DEEP LEARNING

TIANFU HUANG*, ZHIWU WU†, WEN ZHAN‡, CHUNGUANG WANG§ AND TONGYAO LIN¶

Abstract. The measuring accuracy of the electric energy meter, voltage transformer and current transformer shows a dynamic state under the influence of its factors and external factors. The error of the voltage transformer and current transformer cannot be measured by traditional method. This paper establishes a multidimensional error analysis and fault diagnosis system for power metering based on Hadoop architecture and Spark memory calculation. The platform extracted the error signal from the measurement data and calculated the characteristic value of the error signal. Then, dependent cloud and dynamic time rules are used to estimate the transformer's and voltage transformer's continuity. Then, a half-step membership degree cloud generation algorithm is constructed to overcome the error bias randomness and fuzzy characteristics under the influence factors. Finally, the system uses the dynamic correction method to estimate the similarity of error timing and quantitative factors to realize the error calculation of the current transformer and voltage transformer. The power metering error processing system was built with the support of Hadoop and Spark. The timing increment is introduced in the process of data collection. Dependent cloud and dynamic time-repair methods can improve the accuracy of diagnosing errors in electric energy metering. The parallel optimization of big data platforms by belonging to the cloud and dynamic time-warping algorithm is verified.

Key words: Deep learning; Energy metering error; Affiliated cloud; Dynamic time warping; System Estimation

1. Introduction. Power is essential to our country's economy and People's Daily lives. The key to national construction and development is modernizing information construction and management. It is necessary to study all kinds of errors in electric energy measurement systems and reduce their influence as much as possible. Compared with the previous calibration equipment, the multi-purpose electronic calibration equipment has more functions, better performance and higher intelligence. This method has high advantages in the accuracy and speed of inspection. The multiple meter calibration equipment developed and put into operation by the State Grid in 2015 can verify multiple units of measurement at the same time. The measurement accuracy can reach 0.01 magnitude. Literature [1] elaborated on the failure causes of electronic watt-hour meters from internal circuit structure, external humidity sensitivity and chip packaging technology and proposed corresponding countermeasures. Literature [2] uses OOK dynamic test signal modeling combined with the Monte Carlo method to study the error characteristics of digital watt-hour meters. The functional relationship between the factors and the resultant results is examined. The measuring accuracy of the energy meter, voltage transformer and current transformer shows a dynamic state under the influence of its factors and external factors. Reference [3] calibration of frequency multiplier resonance equipment with calibration electrode.

At the same time, the corrected multiplier is used to calculate the correction factor together with the measured output voltage and equivalent resistance. A correction factor is introduced to optimize the uncertainty caused by the resonance effect. In this way, a contactless electrostatic voltmeter calibration scheme is realized. At the same time, the power and quantity errors of different voltage and current are simulated respectively under sinusoidal and non-sinusoidal conditions. The real-time monitoring of the energy meter and the secondary loop is realized [4]. Traditional methods cannot measure the voltage transformer and current transformer error. The measurement error is estimated by the extrapolation method. But this calculation only involves secondary loads, primary currents and primary voltages. Ambient temperature, applied electric and magnetic fields, and

---
*Marketing Service Center of State Grid Fujian Electric Power Co., Ltd., Fuzhou, Fujian, 350013, China (Corresponding author, `m18650869579@163.com`)
†Marketing Service Center of State Grid Fujian Electric Power Co., Ltd., Fuzhou, Fujian, 350013, China
‡Marketing Service Center of State Grid Fujian Electric Power Co., Ltd., Fuzhou, Fujian, 350013, China
§Marketing Service Center of State Grid Fujian Electric Power Co., Ltd., Fuzhou, Fujian, 350013, China
¶Marketing Service Center of State Grid Fujian Electric Power Co., Ltd., Fuzhou, Fujian, 350013, China
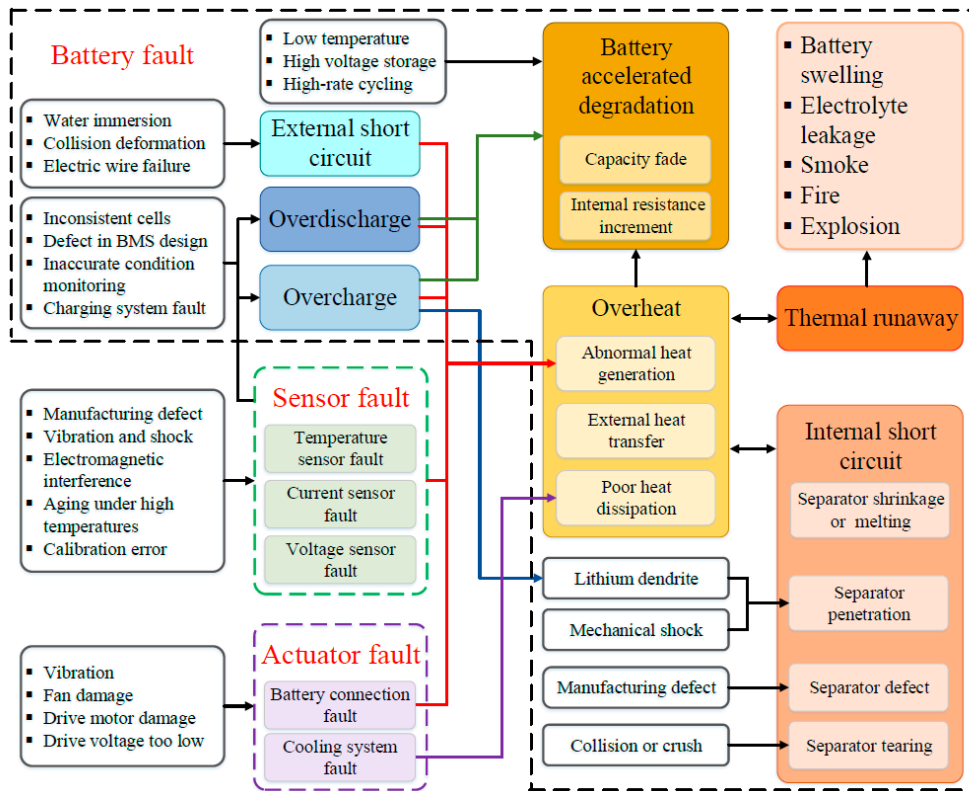
Fig. 2.1: Fault diagnosis method of electric energy metering error information.

leakage current affect the measurement results. The influence of each factor on the measurement result is random and fuzzy. Therefore, in this paper, dependent cloud and dynamic timing algorithms are used to continuously estimate the current and voltage transformer's ratio and phase errors. A half-step membership cloud generation algorithm is constructed [5]. The purpose is to overcome the error bias, randomness, and fuzzy characteristics under the influence of various factors.

2. Digital energy metering analysis based on big data. An error detection method of electric energy metering based on big data is proposed. Hive is selected as the data warehouse management method in this project. Spark computing architecture's efficient characteristics are used to research fast storage of energy metering errors, efficient calculation and distributed parallel optimization for big data [6]. The organic integration of Hadoop and Spark can improve the storage capacity, parallel optimization processing and computing speed of large-scale measurement data. The electric energy measurement error measurement method based on big data is proposed. The system mainly includes four parts: data acquisition, storage and calculation, analysis and diagnosis, and engineering application.

As shown in Figure 2.1 (Picture quoted from Advanced Fault Diagnosis for Lithium-Ion Battery Systems), the system's primary function is to collect, clean, transform and encapsulate the collected information in real time. Among them, Hadoop and Spark are used as carriers to achieve adequate storage of massive data. The characteristic values of electric energy measurement errors are extracted in the analysis and diagnosis, and the type diagnosis is realized. In the engineering application, real-time query and fault analysis of power measurement data is realized. The units showed a strong correlation in the test. Each stage from data collection to actual project implementation is the support and guarantee of subsequent work. The collection and storage of data is the prerequisite for accurate analysis of measurement results [7]. The centre of measurement error is analytic diagnosis. The measurement error calculation method is to show the measurement results to the user.
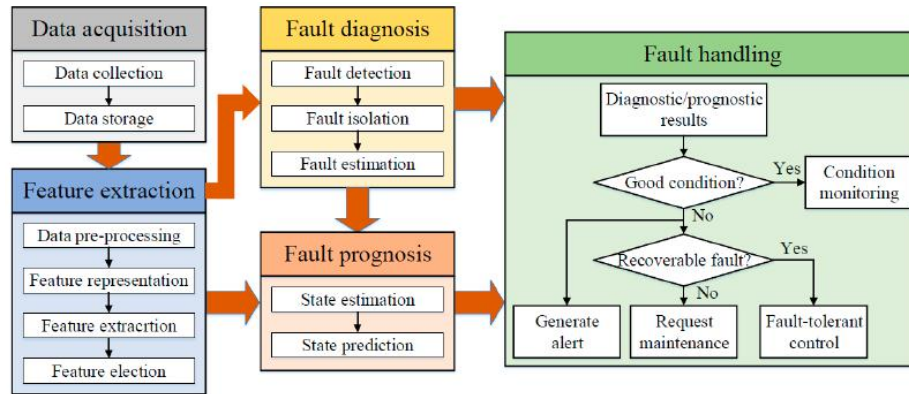
Fig. 2.2: Data processing flow of electric energy metering error.

The error analysis process of electric energy measurement is shown in Figure 2.2.

The Kettle cluster mode is selected during data entry. The work of multiple data collection devices is synchronized and distributed to each PC in the cluster. When the device status is upgraded, not only must the device status data file table be entered into the database, but also the upgraded device file data information must be upgraded. In this way, it is possible to complete the periodic incremental input of data information for various energy metering equipment [8]. As the underlying platform, Hadoop can store a large amount of energy-metering data at high speed. The distributed Spark algorithm can quickly and efficiently process intra-cluster resources and ensure the algorithm's accuracy. The parallel optimal algorithm based on Spark can diagnose and analyze the cause of specific faults in power metering devices. The steps to analyze the problems existing in power measurement using big data are as follows:

1. In periodic increments, The Kettle cluster model inputs power-related data from the customer's power information collection system into the big data infrastructure platform.
2. The analysis of error characteristics in power measurement is divided into three categories: transformer error, analog input merging error and digital error. Secondly, the eigenvalues of electrical energy errors are extracted and calculated.
3. The method of slice and rotation is used to analyze and diagnose the multidimensional error characteristic quantity.
4. Using dependent cloud and dynamic time correction methods to diagnose and type judge measurement errors.

3. Measurement error estimation based on affiliated cloud.

3.1. Membership Cloud Theory. The membership degree cloud method is a method that transforms qualitative and quantitative indexes into each other. Suppose σ is a set of ordinary values. S is the qualitative idea, which relates to V. Assume a random embodiment B of type $x \in \sigma$. The correspondence between x and S, σ, is determined by the following formula:

$$\begin{cases} \sigma : v \to [0,1] \\ \forall x \in v, x \to v(x) \end{cases} \tag{3.1}$$

$v(x)$ is the degree of membership of x relative to S. Merging and distributing between $(x, v(x))$ is called a slave cloud. The member cloud describes the qualitative concept with three parameters:

1. The expected value W_x determines the mean value of the member cloud.
2. The entropy value E determines the variation amplitude of the cloud cluster;
3. Super entropy F_e is an important factor affecting the dispersion degree of cloud water droplets. The cloud droplet data is replaced by the reversely owned cloud to obtain the parameters [9]. Backward

dependent cloud uses statistical methods to translate accurate data into two qualitative concepts, W_x, W_n and F_e. The three parameters of $N_s x_{ai}$ samples can be calculated in the following way:

$$
\begin{cases}
W_x = \dfrac{1}{N_a} \sum_{i=1}^{N_a} x_{ai} \\[2ex]
W_n = \dfrac{\sqrt{\pi/2}}{N_a} i = \sum_{i=1}^{N_a} |x_{ai} - W_x| \\[2ex]
F_e = \sqrt{\dfrac{1}{N_a - 1} \sum_{i=1}^{N_a} (x_{ai} - W_x)^2 - W_n^2}
\end{cases}
\tag{3.2}
$$

After judging W_x, W_n and F_e of x_{ai}, the owning cloud distribution of $(x, v(x))$ can be generated from the positively owning cloud cluster. The membership degree $\sigma(x_{ai})$ of x_{ai} to S can be obtained using the parameters W_x and W_n' in fuzzy mathematics. Where W_n' is an arbitrary number, it conforms to the normal distribution [10]. Its expected value is W_n. The standard deviation is F_e. $\sigma(x_{ai})$ has many different functions for x_{ai}, W_x and W_n', and can generate sets of many membership degrees. The semi-trapezoid and semi-normal membership clouds are selected to examine the influence of various factors on the measurement results. A half-step fuzzy mathematical model is established to describe the influence of various parameters on the measurement results.

3.2. Temperature and frequency belong to the cloud. The temperature of the operating environment of the voltage transformer and current transformer is -25℃ to 55℃. The measurement deviation is temperature-independent in the temperature range close to the Calibration. However, the measurement errors in the high and low-temperature regions vary significantly with the increase and decrease of temperature. In this paper, a half-step membership function is established to characterize the influence of atmospheric temperature on the measurement results. Figure 3.1 is a subgroup of measurement errors as a function of temperature [11]. It is A semi-trapezoidal cloud layer, denoted by $S(W_{xR1}, W_{nR1}, F_{eR1})$ and $S(W_{xR2}, W_{nR2}, F_{eR2})$. If the temperature is between W_{xR1} and W_{xR2}, the degree of membership of this error deviation value is 0. Their corresponding membership functions can quantify the two members outside this interval. Using entropy weight W_{nR1}, W_{nR2}, superentropy F_{eR1} and F_{eR2}, a semi-stepped cloud model is constructed to describe the variation amplitude and the dispersion degree of cloud droplets. The following procedure is used to process the hybrid half-ladder dependent cloud algorithm where error deviation produces the surrounding temperature clouds:

1. Generate random values W'_{nR1} and W'_{nR2}, which are normally distributed. $W'_{nR1} \sim N(W_{nR1} \text{and} F^2_{eR1}), W'_{nR2} \sim N(W_{nR2} \text{and} F^2_{eR2})$.
2. Generate random numbers W'_{nR1} and W'_{nR2}, which are normally distributed. $x_{R1} \sim N(W_{xR1} \text{and} W'^2_{nR1}), x_{R2} \sim N(W_{xR2} \text{and} W'^2_{nR2})$.
3. Repeat steps 1 and 2 until $D \times 1$ binding vectors x_R of x_{R1} and x_{R2} and $D \times 1$ binding vectors W'_{nR} of W'_{nR1} and W'_{nR2} are generated.
4. By substituting the values of the surrounding temperature x_R and W'_{nR} into formula (3), the degree of membership of the surrounding temperature x_R for the deviation of the measurement error can be found:

$$
(x_R, W'_{nR})
\begin{cases}
1 - e^{\frac{(x_R - W_{xR2})^2}{2W'_{nR}{}^2}}, & x_R < W_{xR2} \\[2ex]
0, & W_{xR2} \le x_R \le W_{xR1} \\[2ex]
1 - e^{\frac{(x_R - W_{xR1})^2}{2W'_{nR}{}^2}}, & x_R > W_{xR2}
\end{cases}
\tag{3.3}
$$

Using the forward-owning cloud cluster algorithm from step (1) to step (4), D cloud droplets of (x_R, σ_R) can be generated. The distribution of temperature clusters in each region under each error deviation is given. Figure 3 shows the distribution of the owning group when $\begin{array}{l} W_{xR1} = 30°C, W_{nR1} = 10°C, F_{eR1} = 4°C, \\ W_{xR2} = -5°C, W_{nR2} = 5°C, F_{eR2} = 1°C \end{array}$ occurs. Formula (3) is a function with three components. The midpoint here is 0. The left half is in a downward
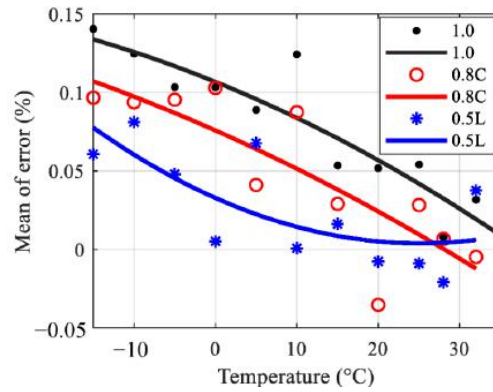
Fig. 3.1: Subordinate cloud distribution of ambient temperature causing error deviation.

trend, and the right half is up until each reach zero. The dependent cloud in Figure 3.1 is a trapezoidal distribution with a broad upper side and a narrow bottom side [12]. The semi-ladder-shaped subordinate cloud in the left region $S(W_{xR1}, W_{nR1}, F_{eR1})$ and the semi-ladder-shaped subordinate cloud rising in the right region $S(W_{xR2}, W_{nR2}, F_{eR2})$ combine to form the hybrid semi-ladder-shaped subordinate cloud in the figure.

It is difficult to obtain the parameters of hybrid semi-trapezoidal dependent cloud in the manufacturers and brands of current transformers and voltage transformers [13]. The above parameters can be obtained from the measured temperature sample data. The measurement result is divided into two parts: (1) the measurement result of the left part is lower than the calibration result; (2) The group on the right contains all other temperature data. The values of $W_{xR2}, W_{nR2}, F_{eR2}$ and $W_{xR2}, W_{nR2}, F_{eR2}$ can be calculated by substituting the temperature sampling data of the two groups on the left and right into equation (2). A half-step fuzzy model is proposed to estimate the effect of atmospheric temperature x_{Rr} on the power measurement results. In the central region $B_R = [x_{Rr} - (F_{eR1} + F_{eR2})/3, x_{Rr} + (F_{eR1} + F_{eR2})/3]$, the deviation of measurement error caused by atmospheric temperature to the number of cloud droplets Z can be expressed as

$$G_R(x_{Rr}) = \frac{\lambda_R G_{\lim}}{Z} \sum_{x_R \in B_R} \sigma_R \tag{3.4}$$

$G = g, \varphi$ is the commutation and phase deviation of the transformer. $G_{\lim} = g_{\lim}, \varphi_{\lim}$ is the corresponding limit value. λ_R is the allowable error range of the measurement result and the ambient temperature range. G is used to replace the R of the subscript in formula (3) and thus $W_{nG1} = W_{nG2} = W_{nG}$ and $W_{nG1} = W_{nG2} = W_{nG}$ to obtain a stepwise dependent cloud, which has a frequency shift relative to the measurement error. The model contains only four parameters: W_{xG1}, W_{xG2}, W_{nG} and F_{eG}. A cloud model based on a positive membership degree is proposed. The membership function should adopt the above symmetric ladder function [14]. The influence of the number of observations on the measurement accuracy is estimated using a symmetrical ladder statistical model.

3.3. Affiliated clouds of other influencing factors. The relationship between the measurement error of the voltage transformer and the external electric field shown in Figure 3.2 can be represented by a rising semi-trapezoidal dependent cloud. Its expression is $S(W_{xW}, W_{nW}, F_{eW})$. The calculation method of the influence of the external electric field on the measurement accuracy is similar to the previous part. The central rain-type cloud system based on gradient is proposed. The member function of $\mu_W(x_W, W'_{nW})$ in the semi-trapezoidal appendage cloud can be expressed as:

$$\mu_W(x_W, W'_{nW}) = \begin{cases} \overset{field}{e^{\frac{(x_W - W_{xW})^2}{2W'_{nW}^2}}}, & x_W < W_{xW} \\ 1, & x_W \geq W_{xW} \end{cases} \tag{3.5}$$
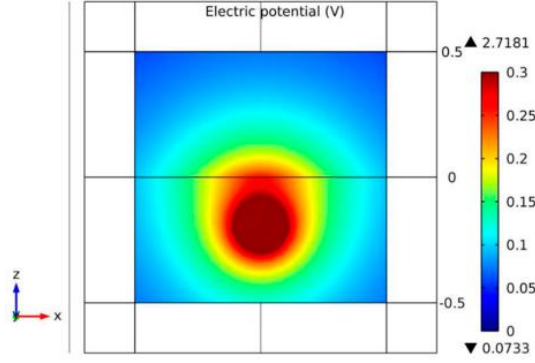
Fig. 3.2: Membership cloud of external electric field measurement error.

x_W and W'_{nW} represent the random number and standard deviation of the electric field cloud drop number, respectively. Previous formula is a fragment function with two parts. The right-hand part is 1. The left paragraph goes from 0 to 1. This causes the degree of membership to change from a discrete growth trend to a continuous saturation state in a specific area of the chart.

The causes of residual magnetism in the transformer core are the breaking of the secondary winding and the sudden drop of current. Therefore, the permeability of the core will be reduced, and the accuracy of the transformer will be affected. The DC component of the residual magnetic field tends to zero with increasing time. Thus, the measurement error of the current transformer is reduced. In this way, the time t_U lost from the most recent current can represent the effect of the remaining magnetic field [15]. The effect of the residual magnetic field on the measurement error deviation is shown in Figure 3.3 with the descending semi-normal dependent cloud cluster. Its expression is $S(W_{xU}, W_{nU}, F_{eU})$. The error is most significant at point t_U. A cloud model based on descending semi-normality is proposed. The membership function $\mu_U(x_U, W'_{nU})$ of the lower semi-normal dependent cloud is shown as follows:

$$\mu_U(x_U, W'_{nU}) = \begin{cases} 1, & x_U \leq W_{xU} \\ e^{\frac{(x_U - W_{xU})^2}{2 {W'_{nU}}^2}}, & x_U > W_{xU} \end{cases} \tag{3.6}$$

x_U is the cloud droplet in the remaining magnetic field. W'_{nU} is a normally distributed random value of the standard deviation. The belonging cloud system with a semi-normal residual magnetic field differs from the one with a semi-stepped magnetic field. As seen from Figure 5, the standard deviation W'_{nU} is expressed in terms of normal distribution. Its expected value and standard deviation are W_{nU}, and the standard deviation is F_{eU}. This allows the dependent cloud to incorporate cloud droplet distribution.

3.4. Similarity between measurement results and factors. Assume that the time series for the measurement error deviation is $x = \{x_1, x_2, \cdots, x_m\}$. The influence factors of voltage transformer are $y = \{y_{X1}, y_{X2}, \cdots, y_{Xm}\}$. $X = R, W, G$ and M stand for temperature, electric field, frequency, magnetic field $y_Y = \{y_{Y1}, y_{Y2}, \cdots, y_{Yn}\}$. The influencing factors of current transformer are. $Y = U, R, M$ and S represent remanence, temperature, magnetic field, and leakage current, respectively. The similarity measurement based on dynamic time warping is also valid for various influencing factors. Figure 6 shows the principle of dynamic time adjustment. The regularization route $k = \{k_1, k_2, \cdots, k_D\}$ is searched from the start point (x_1, y_{Y1}) to the end point (x_M, y_{Yn}). Where k_D represents the optimal structured path of distance $B(x_i, y_{Yj}) = |x_i - y_{Yj}|$, k_{opt} can be chosen to minimize the cumulative distance of dynamic time warping along this path.

$$B_{DTW} = \sum_{k_{opt}} B(x_i, y_{Yj}) = \min(\sum_{k=1}^{D} k_k) \tag{3.7}$$
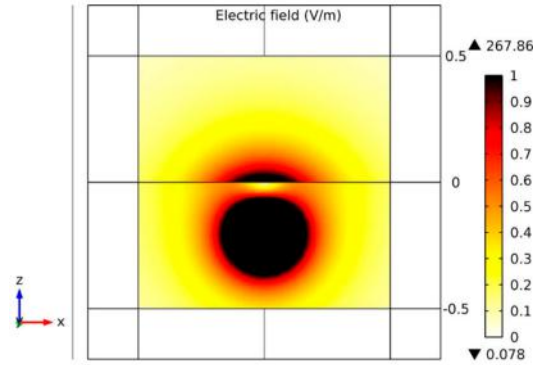
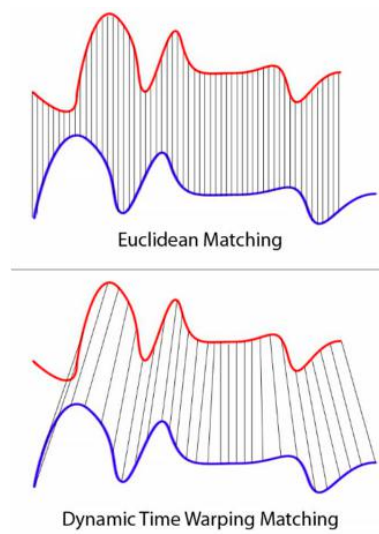Fig. 3.3: Membership cloud of remanent magnetic measurement error.

Fig. 3.4: Dynamic time warping of time series.

A self-repeating algorithm based on time series data is proposed. However, if you repeat it too much, either horizontally or vertically, the fragment shown in Figure 3.4 will not match the other longer fragments. The traditional dynamic time correction methods add gradient restriction to compensate for this shortcoming. A modified rule path by constraining self-repeating on any node. There are the following constraints on the improvement of dynamic time adjustment method:

1. Boundary conditions of regularized paths: $k = \{k_1, k_2, \cdots, k_k\}, k_1 = B(x_1, y_{Y1}), k_k = B(x_m, y_{Y_n})$;
2. The monotonic condition is as follows: when $k_{k-1} = B(x_{i\prime}, y_{Yj\prime})$ and $k_k = B(x_i, y_{Yj})$, $i - i\prime \geq 0, j - j\prime \geq 0$ and $i - i\prime + j - j\prime \neq 0$.
3. Continuity condition: $i - i\prime \leq 1, j - j\prime \leq 1$ when $k_{k-1} = B(x_{i\prime}, y_{Yj\prime})$ and $k_k = B(x_i, y_{Yj})$.
4. The slope restriction conditions are:

$$0 \leq A = \frac{\max(S_{xm}, S_{yn})}{S_{\lim}} < 1 \tag{3.8}$$

S_{xm} and S_{yn} represent the automatic copy time in vertical $(i - i\prime = 0)$ and horizontal $(j - j\prime = 0)$, respectively. $S_{\lim}$ is for persistent limit. A is the tilt factor of the critical value. Points within the

restricted area may not be considered. They are on an unwanted, twisted trajectory. In the closed region, the slope constraint can write the set of points in B_ε as:

$$B_\varepsilon = \begin{cases} B(x_i, y_{Yj}) | S_{\lim} \leq i \leq m, 0 \leq j \leq \left\lceil \dfrac{i - S_{\lim}}{S_{\lim}} \right\rceil \\ or \ S_{\lim} \leq j \leq n, 0 \leq i \leq \left\lceil \dfrac{j - S_{\lim}}{S_{\lim}} \right\rceil \end{cases} \tag{3.9}$$

$\lceil . \rceil$ is the upper bound function. The distance $B(x_i, y_{Yj})$ in the B_ε region is replaced by a larger constant $B_{\max}$ to minimize the cumulative distance of the optimal regularization route so that the points in the restricted region are found on the optimal regularization route. The cumulative distance from point (x_1, y_{Y1}) to (x_i, y_{Yj}) on the optimal regular route is defined as $S(i, j)$. The recursive formula for the cumulative distance $S(i, j)$ is as follows:

$$S(i, j) = B(x_i, y_{Yj}) + \Delta B \tag{3.10}$$

ΔB is the distance accumulated in front of the point (x_i, y_{Yj}). It depends on the number of self-repeats S_{xm} and S_{yn} make in succession along both vertical and horizontal lines. The recursive formula can improve the dynamic time adjustment and find the optimal regular route to achieve the shortest cumulative distance. At this point, an improved dynamic time adjustment scheme is obtained:

$$B_{MDTW} = S(m, n) \tag{3.11}$$

4. Test and result analysis.

4.1. Establishment of test environment and collection of sampling data. Two hosts are used as cluster hosts. The other eight are normal. The two central nodes are "one active, one standby" cases. The data storage system mainly completes the storage, management and scheduling of test data. The latter is to ensure the reliability of the cluster system. Select CentOS6.4 as the operating system. Maximize your use of the /home directory. The experimental case data is obtained from the primary platform file of the power measurement equipment. The Kettle software is used to preprocess data and then input all data into the Hive data warehouse. After analysing the fault intelligently, the Spark SQL model queries and displays the fault in real-time.

4.2. Research on Multidimensional Testing Methods. The fault diagnosis system of electric energy measurement error analysis is constructed. Since the operation rate and accuracy of the algorithm are directly related to the overall effect of the entire power measurement error analysis, the test results of the speed and accuracy of the proposed scheme's power measurement error feature extraction are listed in Table 4.1.

By analysing the data of different fault categories, the fault diagnosis effect of the proposed method based on cloud ownership and dynamic time correction is further verified. At the same time, the accuracy of the power measurement error extensive data analysis system is judged. The diagnostic conclusions of the analysis are shown in Table 4.2.

Table 4.2 lists five typical errors in electrical energy measurement. There are 100 experimental data. The experiment was carried out in single-machine mode and cluster mode. When the number of test cases is larger, the accuracy of the test can reflect the true degree of test error. True diagnostic results were obtained from 100 test data (Figure 4.1)). The solid lines on the left represent each of the five error types from R1 to R5. The dotted line on the right clearly represents the error type's diagnostic accuracy. The fault diagnosis accuracy of post-cluster methods using dependent cloud and dynamic time-repair methods differs significantly from that of a single method. The identification accuracy of R2 error in cluster mode is significantly higher than that in single-machine mode. The experimental results show that the dependent cloud and dynamic time repair method can improve the accuracy of diagnosing the types of energy metering errors. The parallel optimization of big data platforms by belonging to the cloud and dynamic time-warping algorithm is verified.

Table 4.1: Test and verification results of calculation of error eigenvalues.

Error information evaluation index	The electric energy meter reversed	Electric energy meter stalls	Electric energy meter spinning
Record time	2022.08.01	2022.09.01	2022.108.01
Output records (strips)	8	356	9
Time (s)	5.994	3.731	1.410
verify	Table number is 31139	The table code is 28313	The table code is 30382
	The table code of 2022.07.03 is 10.03	PAP_R=0.02 on 2022.09.01. PRP_R=1.10	RUN_CAP=23958
	The table code of 2022.08.01 is 0.0	PRP_R =0.00 on 2022.09.02. PRP_R=0.00	PRP_E=415333
Verify conclusion	It is verified that the electric energy meter is running backward, and the conclusion is correct.	It is verified that the electric energy meter has stopped, and the conclusion is correct.	It is verified that the electric energy meter is flying, and the conclusion is correct.

Table 4.2: Test and verification results of calculation of error eigenvalues.

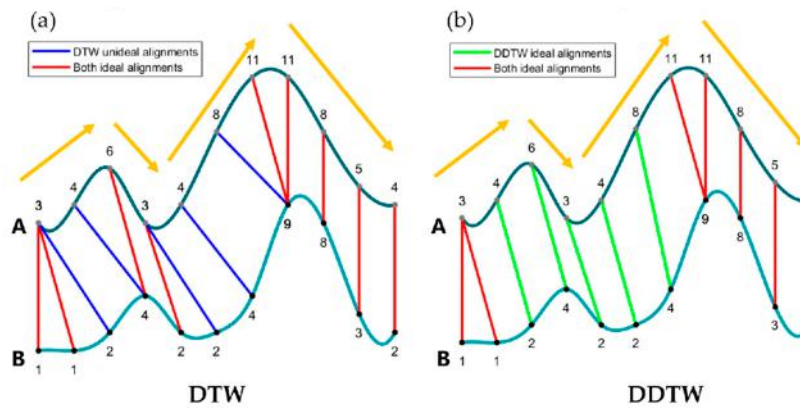| Error type	ID
The transformer is improperly connected	R1
The collection device is disconnected	R2
The energy meter is incorrectly connected	R3
Analog input combined cell quantization error	R4
Normal state	R5

Fig. 4.1: Comparison of accuracy rates of membership cloud and dynamic time warping diagnosis under two modes.

5. Conclusion. In this paper, the deviation problem of digital electric energy measurement is discussed in detail from the transfer of sample value, the input and combination of analogy quantity, the measurement error of digital electric energy meter and their effect on electric energy measurement. The power metering error

processing system is constructed with the support of Hadoop and Spark. The timing increment is introduced in the process of data collection. The flexible distributed database based on Spark architecture is used to solve the problem quickly, and the error characteristic of the system is obtained. The power metering extensive data analysis system based on the owning cloud and dynamic timing restoration is constructed to optimize real-time data. At the same time, it can also be used to diagnose all kinds of faults in electric energy measurement. The experiment proves that an effective distributed data processing method is realized on the big data platform.

REFERENCES

[1] Yu, X., Zheng, D., & Zhou, L. Credit risk analysis of electricity retailers based on cloud model and intuitionistic fuzzy analytic hierarchy process. International Journal of Energy Research, 2021;45(3): 4285-4302.

[2] Asres, M. W., Ardito, L., & Patti, E. Computational cost analysis and data-driven predictive modeling of cloud-based online-NILM algorithm. IEEE Transactions on Cloud Computing, 2021; 10(4): 2409-2423.

[3] Tajalli, S. Z., Kavousi-Fard, A., Mardaneh, M., Khosravi, A., & Razavi-Far, R. Uncertainty-aware management of smart grids using cloud-based lstm-prediction interval. IEEE Transactions on Cybernetics, 2021;52(10): 9964-9977.

[4] Geng, Y., Pan, F., Jia, L., Wang, Z., Qin, Y., Tong, L., & Li, S. UAV-LiDAR-based measuring framework for height and stagger of high-speed railway contact wire. IEEE Transactions on Intelligent Transportation Systems, 2021; 23(7): 7587-7600.

[5] Koivumäki, P., Steinböck, G., & Haneda, K. Impacts of point cloud modeling on the accuracy of ray-based multipath propagation simulations. IEEE Transactions on Antennas and Propagation, 2021; 69(8): 4737-4747.

[6] Tran, M. K., Panchal, S., Chauhan, V., Brahmbhatt, N., Mevawalla, A., Fraser, R., & Fowler, M. Python-based scikit-learn machine learning models for thermal and electrical performance prediction of high-capacity lithium-ion battery. International Journal of Energy Research, 2022; 46(2): 786-794.

[7] Yang, L., Yu, K., Yang, S. X., Chakraborty, C., Lu, Y., & Guo, T. An intelligent trust cloud management method for secure clustering in 5G enabled internet of medical things. IEEE Transactions on Industrial Informatics, 2021; 18(12): 8864-8875.

[8] Miller, C., Picchetti, B., Fu, C., & Pantelic, J. Limitations of machine learning for building energy prediction: ASHRAE Great Energy Predictor III Kaggle competition error analysis. Science and Technology for the Built Environment, 2022; 28(5): 610-627.

[9] Ghafari, R., Kabutarkhani, F. H., & Mansouri, N. Task scheduling algorithms for energy optimization in cloud environment: a comprehensive review. Cluster Computing, 2022; 25(2): 1035-1093.

[10] Pretto, S., Ogliari, E., Niccolai, A., & Nespoli, A. A new probabilistic ensemble method for an enhanced day-ahead pv power forecast. IEEE Journal of Photovoltaics, 2022; 12(2): 581-588.

[11] Azimi Nasab, M., Zand, M., Eskandari, M., Sanjeevikumar, P., & Siano, P. Optimal planning of electrical appliance of residential units in a smart home network using cloud services. Smart Cities, 2021; 4(3): 1173-1195.

[12] Saxena, D., Gupta, I., Singh, A. K., & Lee, C. N. A fault tolerant elastic resource management framework toward high availability of cloud services. IEEE Transactions on Network and Service Management, 2022; 19(3): 3048-3061.

[13] Alam, T. Cloud-based IoT applications and their roles in smart cities. Smart Cities, 2021; 4(3): 1196-1219.

[14] Mansour, R. F., Alhumyani, H., Khalek, S. A., Saeed, R. A., & Gupta, D. Design of cultural emperor penguin optimizer for energy-efficient resource scheduling in green cloud computing environment. Cluster Computing, 2023; 26(1): 575-586.

[15] Belgacem, A., & Beghdad-Bey, K. Multi-objective workflow scheduling in cloud computing: trade-off between makespan and cost. Cluster Computing, 2022;25(1):579-595.